J Mater Sci (2007) 42:7708–7715
DOI 10.1007/s10853-007-1675-x

Evolution of elastic mechanical properties during pressureless sintering of powder-processed metals and ceramics

Hugh Alan Bruck · Yasser M. Shabana · Buli Xu · JonPaul Laskis

Received: 2 August 2005 / Accepted: 8 March 2007 / Published online: 3 June 2007

Abstract Metal and ceramic structures are being fabricated by pressureless sintering of compacted powders. As the powdered compacts are sintered, the pore volume fraction, generally referred to as porosity, decreases while the elastic mechanical properties increase. In this investigation, a new relationship is drawn between porosity and the evolution of elastic mechanical properties in pure ceramic and metal specimens. To develop this relationship, disk specimens are prepared from Nickel and Alumina powders, then sintered to different temperatures. The evolution of porosity is then evaluated from density measurements, while the corresponding elastic mechanical properties are measured using the ultrasonic wave propagation technique. These experimental measurements are compared with several different descriptions: (1) a conventional power law formula, (2) a quadratic formula, (3) a numerical micromechanical porosity simulation, and (4) a new empirical formula that combines the effects of evolving particle cohesion on the elastic properties of the matrix material and the reduction of these properties due to porosity. For the Young's modulus, the new empirical formula provides a better description than the alternative formulas. In the case of Poisson's ratio, similar conclusions could be made. However, the Poisson's ratio exhibited a different sensitivity to particle cohesion that was more directly related to the evolution of particle cohesion.

H. A. Bruck (✉) · Y. M. Shabana
Department of Mechanical Engineering, University of Maryland, College Park, MD 20742, USA
e-mail: bruck@umd.edu

B. Xu · JonPaul Laskis
Department of Mechanical Engineering, University of South Carolina, Columbia, SC 29208, USA

Y. M. Shabana
Mechanical Design Department, Faculty of Engineering, Helwan University, El-Mataria, P.O. Box 11718, Cairo, Egypt

Introduction

Metal and ceramic structures, such as Functionally Graded Materials (FGMs), are being fabricated by compacting and sintering metal and ceramic powders [1]. When sintering the powdered compacts, the pore volume fraction, generally referred to as porosity, will decrease with increasing temperature and time, leading to shrinkage. For FGMs, stress will be induced due to differences in the evolution of shrinkage throughout the composition gradient, which can lead to cracking and/or debonding if the local strength within the composition gradient does not evolve more quickly than the shrinkage stress. This damage may be avoided by optimizing the geometry and/or gradient architecture of the sintered component. This optimization can be achieved through Finite Element Analysis (FEA) models of the sintering behavior. To develop these models, it is necessary to accurately describe the evolution of mechanical properties during the sintering process. In particular, the evolution of the elastic mechanical properties, Young's modulus and Poisson's ratio, needs to be characterized. During sintering, the porosity will be consumed as the sintering temperature and sintering time increases, leading to volumetric shrinkage and a corresponding increase in density. It has been determined that mechanical properties of porous materials can depend directly on the relative density, and corresponding empirical formulas have

been developed to describe the evolution of these properties in order to study the evolution of stress during sintering without direct experimental verification of the property evolution [2–5]. Some studies [3–8] have also considered the contribution of viscosity effects on the sintering behavior, however the assumed evolution of mechanical properties has still not been verified. Therefore, it is important to directly characterize the evolution of mechanical properties during sintering as a function of porosity or relative density.

Many experimental techniques have been used to measure the material properties of a sintered component. Ultrasonic sound wave propagation, which is a nondestructive technique, is a common technique for measuring some of the mechanical properties such as Young's modulus and Poisson's ratio. Ultrasonic measurements of the elastic constants for Hot Isostatically Pressed (HIP) metal-ceramic composites used in the fabrication of FGMs have been previously investigated for determining the level of damage induced during processing, as well as the effects of damage on mechanical properties [9]. Comparison of measured mechanical properties with formula predictions has revealed that the presence of particle damage causes substantial deviation from the expected behavior. A comprehensive set of values for the major properties of the sintered α-Alumina as a function of the sintering temperature has also been measured [10].

The characterization of properties in previous research efforts has been carried out after the materials had been sintered to temperatures sufficient to minimize porosity. However, it is important to characterize the evolution of porosity and mechanical properties during sintering. In this research investigation, circular disks are fabricated from Nickel and Alumina powders commonly used as model materials for studying the powder processing of FGMs. These disks are then sintered to different temperatures in order to measure the evolution of porosity and mechanical properties as the porosity is consumed. The density is initially evaluated by measuring the mass and volume of each sample. Using the measured density, elastic mechanical properties such as Young's modulus and Poisson's ratio can be experimentally determined through ultrasonic sound wave propagation. These experimental measurements are compared with a conventional power law description and a new empirical formula that combines the effects of the evolving particle cohesion on the elastic mechanical properties of the matrix material and the reduction of these properties due to porosity. Direct experimental verification of these formulas enables them to be accurately employed in FEA models of sintering stresses in components made of metal and ceramic powders, as well as FGMs made from these constituents.

Characterization of elastic mechanical properties using ultrasonic sound wave propagation

There are many techniques for measuring the elastic mechanical properties of materials. A very accurate method utilizes the propagation characteristics of ultrasonic waves. Ultrasonic waves are waves that are produced above 20 KHz, which cannot be heard by the human ear. There are several types of ultrasonic wave measurements that are practiced. The most common types of waves are longitudinal and shear or transverse waves. Longitudinal waves are compressive waves in which the particle of motion travels in the same direction of wave being propagated. The other most common wave type is called shear waves in which the particles oscillate perpendicular to the direction of the wave propagation. Both types of waves are shown in Fig. 1a.

These waves can be used to non-destructively characterize the elastic mechanical properties in materials. In order to create these ultrasonic waves, transducers are used to convert electrical energy into mechanical energy in the form of sound. A transducer is made up of three core components: active element, wear plate and backing. The

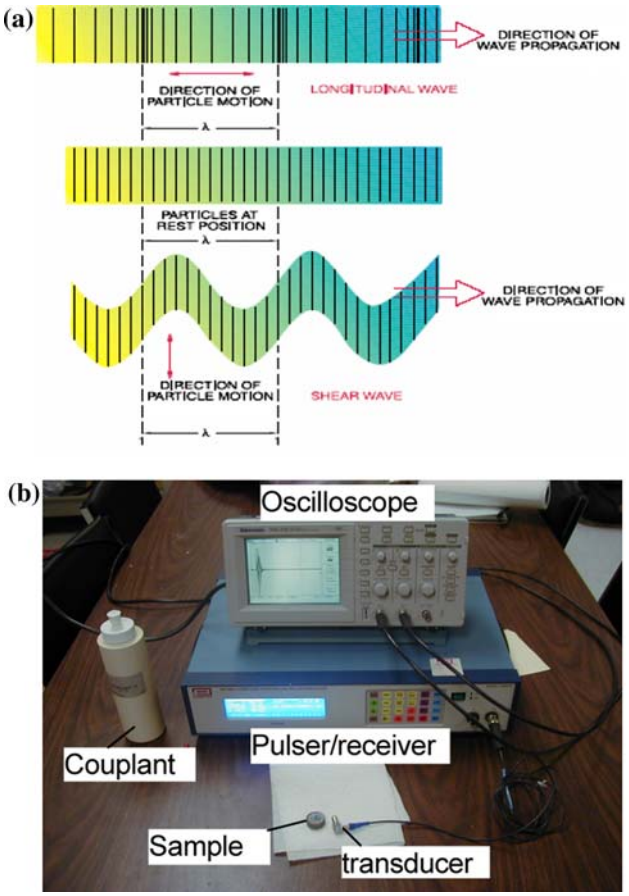

Fig. 1 (**a**) Illustration of longitudinal and shear waves, and (**b**) experimental setup for wave velocity measurement

active element is most vital component of the transducer because it is responsible for converting electrical energy into ultrasonic vibrations. This vibration is controlled by the backing which is a high density material that absorbs the vibration energy created from the back face of the active element. In order to protect the active element from being damaged a wear plate is located in the front of it.

Once the active element is energized, waves project from the transducer into the elastic medium. These sub-sound waves are reflected off the back surface of the material and are converted back into a signal that is read by the piezoelectric receiver. With the knowledge of this time interval or time of flight (TOF) and the material thickness, the wave traveling velocity in this material can be determined. Using these velocity calculations, a variety of material properties such as Poisson's ratio and Young's modulus can be calculated as follows

$$v = \frac{1 - 2(V_T/V_L)^2}{2 - 2(V_T/V_L)^2} \quad (1)$$

Table 1 System parameters used for ultrasonic sound wave velocity measurements

Parameter	Value for Longitudinal Wave Measurements	Value for Shear Wave Measurements
PRF	500 Hz	500 Hz
Energy	16 μJ	32 μJ
Damping	50 Ω	16 Ω
Attenuation	22 dB	0.5 dB
Gain	40.0 dB	26 dB

$$E = \frac{\rho V_L^2 (1 + v)(1 - 2v)}{(1 - v)} \quad (2)$$

where, V_L and V_T are the velocities of the longitudinal and shear waves, respectively. The material properties ρ, E, and v are the density, Young's modulus, and Poisson's ratio, respectively.

Wave velocities for the disks were measured using a 200 MHz Computer Controlled Pulser/Receiver (CCPR) model 5900 PR, a Tektronix TDS 210, 2-channel Oscilloscope, a Panametric 2 MHz longitudinal wave transducer and a Panametric 5 MHz shear wave transducer (Fig. 1b). The system was calibrated using a steel step gauge, which resulted in the system parameters seen in Table 1.

One drop of ultrasonic Couplant D gel (longitudinal wave couplant) was applied to the flat surface of each specimen for longitudinal wave velocity measurements, and a more viscous Shear Wave Couplant (SWC) was used for the shear wave velocity measurements. This type of gel is used to maximize sound coupling on rough surfaces where the transducer cannot make an even contact with the sample surface. Once this gel is applied, the transducer was placed in the couplant on top of the sample. It is held in place until the waves observed on the oscilloscope become stabilized. Figure 2a and c show the basic waveforms from the longitudinal wave transducer and shear wave transducer respectively without samples. Then once the couplant is applied to the elastic medium, the transducer is placed on top and small peaks are observed (Fig. 2b, d). At this point, the distance between the highest peak of the first wave to the highest peak of the second wave is measured. The average time of flight of the sound wave is obtained from this measurement, which is then used to calculate the

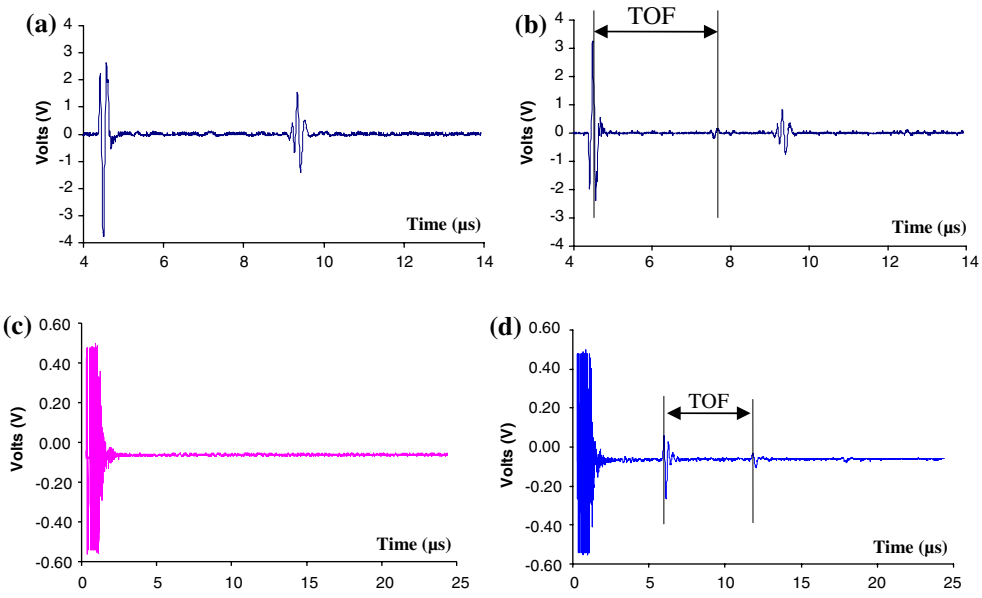

Fig. 2 Waveforms from ultrasonic transducers: (**a**) waveform from longitudinal wave transducer without sample; (**b**) waveform from longitudinal wave transducer with sample N3; (**c**) waveform from shear wave transducer without sample; (**d**) waveform from shear wave transducer with sample N3. Sample N3 is the nickel sample sintered to 950 °C

wave velocity by dividing it into the distance of flight, which is twice the disk thickness.

Specimen preparation

Metal and ceramic disks for wave velocity measurements were prepared from Nickel and Alumina powders with mean diameters of 3 and 0.4 μm, respectively. A binder, Q-PAC 40, was added to the Alumina disks by the amount of 0.035 weight fraction. All specimens were cold pressed to 70 MPa in a steel die to form the powder compact. The densities of the disks were experimentally calculated by measuring the volume and weight of each sample. The dimensions of each sample (diameter and thickness) were measured at 4 different locations using a Mitutoyo Dogmatic Caliper with an accuracy of 0.001 mm. Once the dimensions of the samples are recorded, each sample was weighed using an electronic scale with an accuracy of 0.001 g.

Specimens were sintered to peak temperatures of 550, 750, 950, 1100, and 1350 °C using thermal profile shown in Fig. 3. The specimens were rapidly air cooled after reaching the peak temperature to minimize additional sintering effects. Examples of the metal and ceramic sintered specimens can be seen in Fig. 4. The measured linear shrinkage variations with the sintering temperature for nickel and alumina samples are shown in Fig. 5. The relative density, $\bar{\rho}$, was calculated using the following equation:

$$\bar{\rho} = \frac{\rho}{\rho_{theoretical}} \tag{3}$$

Where $\rho_{theoretical}$ is the theoretical density for a fully dense material, and(ρ is the current density. Results from these calculations can be seen in Fig. 6.

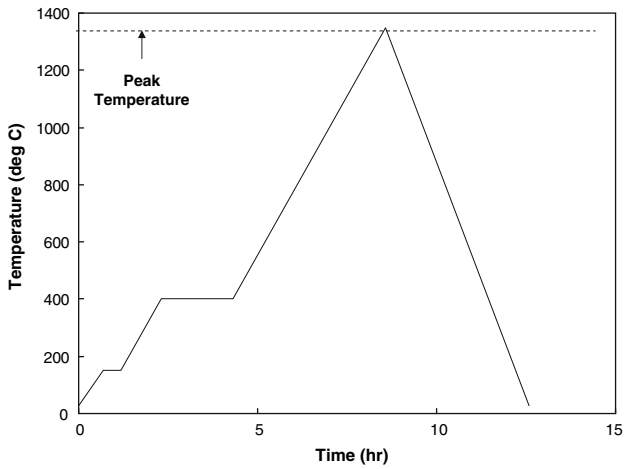

Fig. 3 Thermal profile for the sintering process

Fig. 4 Pure Alumina and pure Nickel disk specimens

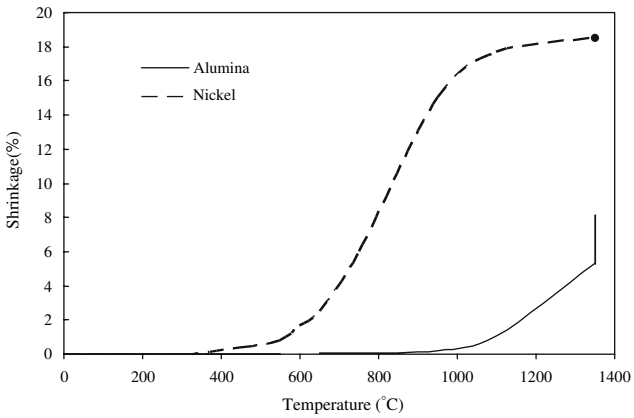

Fig. 5 Linear shrinkage variation with the sintering temperature

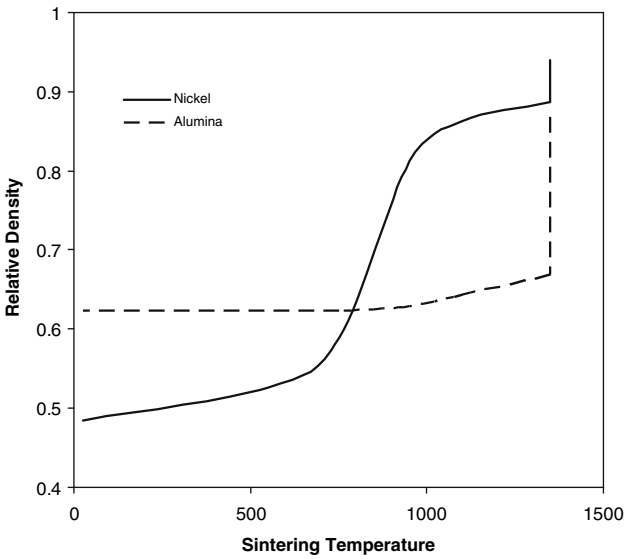

Fig. 6 Variation of the relative density with the sintering temperature

Experimental results and formulae for the evolution of elastic mechanical properties

Using the measured densities with the shear and longitudinal wave velocity measurements, the elastic mechanical properties were calculated from Eqs. 1 and 2. The values obtained from these calculations can be seen in Table 2. The values are also shown for the unsintered specimens, whose mechanical properties are essentially nonexistent in comparison to the sintered specimens and result in effectively no wave velocity.

Young's modulus

Previous research has been conducted on relating the Young's modulus for fully cohesive sintered materials to the amount of porosity present in the materials. Pabst and Gregorova [11], developed an empirical description where the Young's modulus is a quadratic function of the relative density as follows,

$$E = E_0\,\bar{\rho}^2 \tag{4}$$

where E_0 is the Young's modulus for the fully dense material. An alternative formula has also been proposed to allow for a vanishing modulus at a porosity less than 1 [12],

$$E = E_0\left(\frac{\bar{\rho}-\bar{\rho}_1}{1-\bar{\rho}_1}\right)^m \tag{5}$$

where m and $\bar{\rho}_1$ are constants. Using this formula, numerical micromechanical simulations of porosity have been used to determine values of these constants based on different pore structures [13]. The microstructure for the sintered materials in this investigation can be seen in Fig. 7, obtained at high resolution with an AFM for the fine Alumina specimens, and at lower magnifications using an optical microscope for the coarser Nickel specimens. From this figure, it appears that by 1350 °C, the Alumina particles have begun to sinter together to form larger spherical pores. Similarly, the Nickel has almost completely sintered with only spherical pores remaining. Thus, the pore structure for both materials is best described by overlapping spherical pores. For this microstructure, the parameters in Eq. 5 were determined from the numerical simulations to be $\bar{\rho}_1 = 0.182$ and m = 1.65. Equation 4 has also been generalized to describe the Young's modulus for porous materials as they are sintered by using an arbitrary exponent as follows [2],

$$E = E_0\bar{\rho}_s^z \tag{6}$$

where z is the power law exponent reflecting a sensitivity to the pore structure, and $\bar{\rho}_s$is the sintered relative density.

During the sintering process the cohesion between the particles evolves due to diffusion along the particle-particle boundaries. Therefore, it is more realistic to consider the evolution of particle cohesion when describing the evolution of elastic mechanical properties during sintering. The evolution of particle cohesion is directly related to the diffusion-controlled consumption of particle-particle interfaces, typically described a Weibull power law time-dependent exponential equation, consistent with the Kolmogorov-Johnson-Mehl-Avrami kinetic theory of nucleation and growth. However, it is assumed that the consumption of particle-particle interfaces is directly related to the change in relative density. Therefore, the change of relative density can be substituted in place of time in the exponential relation, and the effects of evolving particle cohesion can be combined with the effective of

Table 2 Evolution of elastic mechanical properties measured with ultrasonics

Material	Temp. (°C) (mm)	Thickness	Longitudinal Velocity (V_L) (m/s)	Shear Velocity (V_T) (m/s)	Density (kg/m^3)	Poisson's ratio v	Young's modulus E (GPa)
Nickel	1350	8.26	5416	2950	7899	0.29	177
	1100	8.15	5110	2753	7680	0.30	152
	950	8.35	4588	2530	7232	0.28	116
	750	9.04	3107	1808	5240	0.24	43
	550	9.34	2203	1279	4680	0.25	19
	25	9.4	~0	~0	4584	0	0
Alumina	1350	5.11	10298	6173	3530	0.16	346
	1100	7.14	6596	4275	2640	0.14	121
	950	7.52	3686	2558	2535	0.04	35
	750	7.60	2310	1624	2478	0.01	13
	25	7.62	~0	~0	2454	0	0

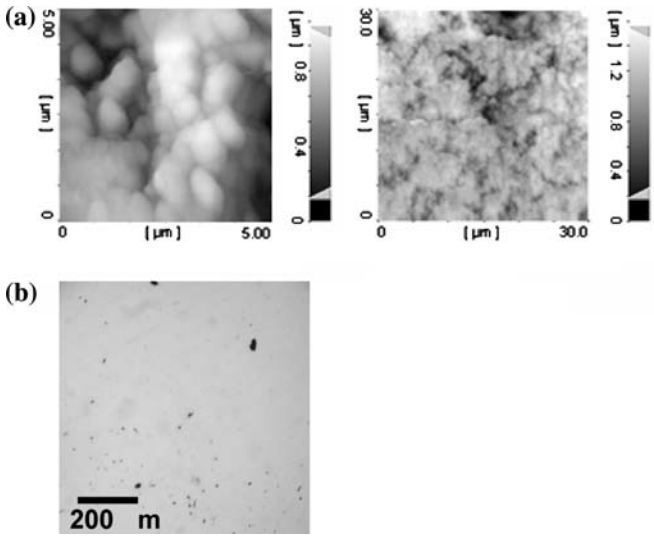

Fig. 7 Micrographs of (**a**) Alumina sintered at 1350 °C obtained with an AFM, and (**b**) Nickel sintered at 1350 °C obtained with an optical microscope. The sintered microstructures indicates that the porosity is best described by overlapping spherical pores for the purposes of describing the evolution of mechanical properties

porosity on the Young's modulus to develop the following new empirical description,

$$E = E_0\left(1 - e^{\left(c\frac{(\bar{\rho}_i - \bar{\rho}_s)}{(\bar{\rho}_s - 1)}\right)}\right)\bar{\rho}_s^2 \tag{7}$$

where, $\bar{\rho}_i$ is the initial relative density and c is a fitting parameter. The first parenthesis in Eq. 6 represents the relative amount of particle cohesion while the second one represents the effect of porosity on the property evolution. If the cohesion effect is omitted, the resulting relation will be the same as Eq. 4.

Figure 8 shows the variation of the Young's modulus for both Nickel and Alumina specimens sintered to different relative densities. The experimental values and the values fit to the power law description and the new empirical formula corresponding to Eq. 7 are shown, as well as the values from Eq. 5 using the constants obtained from the numerical micromechanical simulations and the quadratic formula in Eq. 4. For both descriptions, a fully dense modulus of 400 GPa was used for Alumina and 210 GPa was used for Nickel. In reference [2], values ranging from 0.3 to 4 are reported for the power law exponent z in Eq. 6. For the data presented in Fig. 8, a power law exponent of 3 was found to provide a best fit to the experimental data for both Nickel and Alumina. The new empirical formula was determined to provide a best fit to the experimental data using a value of 5 for the exponential coefficient c in Eq. 7 for both materials. It can be seen from this figure that the experimental results are close to the values obtained from the conventional power law description when the relative density is higher than 68% for Alumina and above 53% for Nickel. When considering the effects of both particle cohesion and porosity, the experimental values agree well with the empirical formula for both Alumina and Nickel at all relative densities.

It can be seen that the values obtained from the quadratic formula and the numerical porosity model are nearly identical, and reasonably correlate with the experimental measurements at relative densities above 0.8. The power law description tends to agree better with the experimental measurements at lower relative densities, but still does not fit as well for small initial changes in relative density. The evolution of the relative amount of particle cohesion obtained from the new empirical formula for Nickel and Alumina can be seen in Fig. 9. It is easy to see that the particle cohesion evolves very rapidly, reaching a value of 50% after approximately a 6% change in relative density.

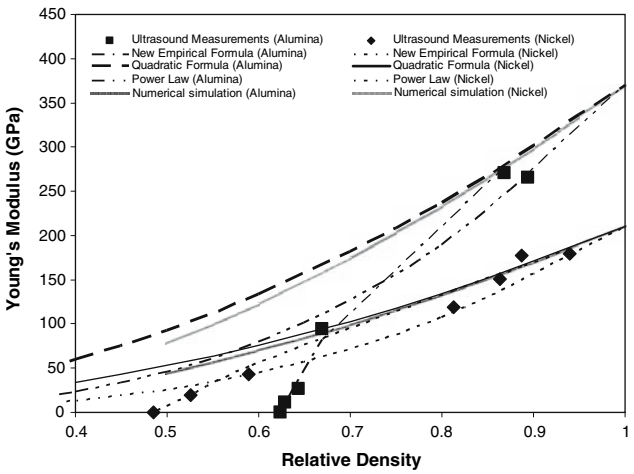

Fig. 8 Evolution of Young's modulus with sintered relative density experimentally measured using ultrasonic sound wave propagation and fit to the conventional power law description in Eq. 5 and the new empirical description in Eq. 6. The values expected for a fully cohesive porous material in Eq. 4 are also plotted for comparison

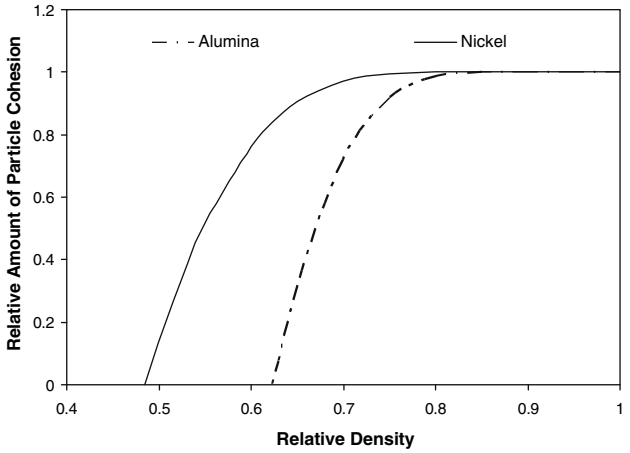

Fig. 9 Relative amount of particle cohesion obtained from the new empirical formula for sintering of Nickel and Alumina powders

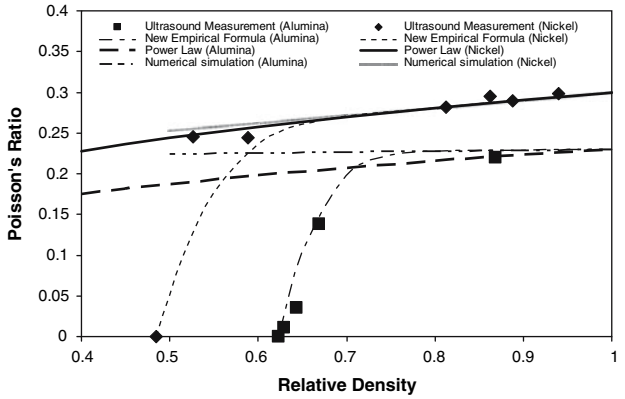

Fig. 10 Evolution of Poisson's ratio with sintered relative density experimentally measured using ultrasonic sound wave propagation and obtained from the conventional power law description in Eq. 7 and the new empirical formula in Eq. 8

This corresponds well with the observed correlation of the power law description to the experimental data, and indicates that power law descriptions are appropriate to describe the evolution of density when the particles in the matrix are mostly cohesive. It is also evident in Fig. 8 by comparing the two descriptions and the experimental data with the values of a fully cohesive porous material obtained from Eq. 4.

Poisson's ratio

The Poisson's ratio is described for the alumina and nickel materials as they are sintered using the same power law relationship given in Eq. 6. Therefore, the power law description for Poisson's ratio is given by,

$$v = v_0 \bar{\rho}_s^{z*} \tag{8}$$

where, v_0 is the Poisson's ratio of the fully dense material and $z*$ is a different constant than used in Eq. 6. Thus, the Poisson's ratio is being treated differently than the Young's modulus. The numerical micromechanical simulations of porosity have also indicated that the following formula can be applied to fully cohesive porous materials [12],

$$v = v_0 + \left(\frac{1-\bar{\rho}_s}{1-\bar{\rho}_1}\right)(v_1 - v_o) \tag{9}$$

where for overlapping spherical pores $\bar{\rho}_1$= 0.16 and v_1 = 0.221. Therefore, the new empirical description for Poisson's ratio can be expressed as follows,

$$v = \left(v_0 + \left(\frac{1-\bar{\rho}_s}{1-\bar{\rho}_1}\right)(v_1 - v_o)\right)\left(1 - e^{\left(c*\frac{(\bar{\rho}_i - \bar{\rho}_s)}{(\bar{\rho}_s - 1)}\right)}\right) \tag{10}$$

where $c*$ is a different constant than used in Eq. 7.

Figure 10 shows the variation of Poisson's ratio for both Nickel and Alumina specimens sintered to different relative densities. The experimental values and the values obtained from the power law description and the new formula corresponding to Eq. 10 are shown. For both descriptions, a fully dense Poisson's ratio of 0.23 was used for Alumina and 0.3 was used for Nickel, while an exponent of 0.3 for sintering materials was used in the power law description and an exponent of 8 in the new formula. It can be seen from this figure that unlike the experimental results for the modulus, Poisson's ratio values obtained from the new formula are much closer than the ones obtained from the power law description with the exception of some of the initial sintering values for Nickel which are closer to the fully cohesive values than the Young's modulus measurements were. The Poisson's ratio fit obtained using numerical micromechanical simulations of porosity for a fully cohesive porous material also appears to be less sensitive to porosity, which indicates the Poisson's ratio normalized by the fully dense value is more directly related to the evolution of particle cohesion than Young's modulus (Fig. 11). From these results, it can be concluded that Poisson's ratio exhibits a different sensitivity to particle cohesion than the Young's modulus during the sintering process.

Conclusions

The evolution of elastic mechanical properties during pressureless sintering of metal and ceramic powders was studied using disk specimens made from Nickel and Alumina powders. These specimens were sintered to different temperatures in order to characterize the elastic mechanical

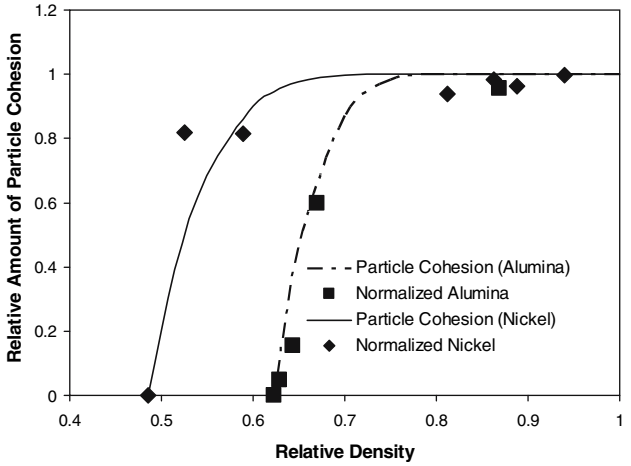

Fig. 11 Comparison of the measured Poisson's ratios normalized by the fully sintered values with the evolution of particle cohesion determined from the new empirical formula indicating the Poisson's ratio is capable of providing more direct insight into the evolution of particle cohesion than Young's modulus

properties at different levels of relative density associated with the pressureless sintering process.

The ultrasonic sound wave propagation technique, an effective non-destructive method for characterizing elastic mechanical properties, was used to measure the Young's modulus and Poisson's ratio from longitudinal and shear wave velocities. These measurements were used to fit a conventional power law description relating the relative density to the elastic mechanical properties, and an alternative description using constants obtained from numerical micromechanical simulations of porosity. A new empirical description was also proposed for describing the evolution of Young's modulus by combining the effects on the load-bearing capacity of the matrix due to diffusion-controlled evolution of particle cohesion and the reduction of this capacity due to the presence of residual porosity through an exponential and quadratic relationship to relative density respectively. Comparisons between the measurements, the power law description, the numerical micromechanical porosity simulations, and the new empirical description indicated that the new empirical description provided a better fit for small initial changes (>6%) in relative density. The corresponding change in particle cohesion is consistent with the correlation of the power law description to the experimental data, and indicates that power law descriptions are appropriate to describe the evolution of density when the particles in the matrix are mostly cohesive.

The new empirical description was also applied to the evolution of Poisson's ratio using just the particle cohesion effects. Comparisons between the measurements, the power law description, the numerical micromechanical porosity simulations, and the new empirical description indicated that the new empirical description provided the best fit. Because the numerical micromechanical porosity simulations indicate Poisson's ratio is less sensitive to porosity, it was determined that Poisson's ratio was more directly related to the evolution of particle cohesion in pressurelessly sintered metal and ceramic powders than Young's modulus. It was also determined that the Poisson's ratio exhibits a different sensitivity to the evolution of particle cohesion than the Young's modulus during the sintering process.

References

1. Winter AN, Corff BA, Reimanis IE, Rabin BH (2000) J Am Ceram Soc 83:2147
2. German RM (1996) Sintering theory and practice. John Wiley and Sons
3. Shinagawa K (2003) JSME Int J Ser A 46:378
4. Shinagawa K (1999) Comp Mater Sci 13:276
5. Zhang B, Gasik M (2002) Comp Mater Sci 25:264
6. Jagota A, Scherer GW (1995) J Am Ceram Soc 78:521
7. Larsson PL, Biwa S, Storakers B (1996) Acta Mater 44:3655
8. Storakers B, Fleck NA, McMeeking RM (1999) J Mech Phys Solids 47:785
9. Bruck HA, Rabin BH (1999) J Mater Sci 34:2241
10. Ronald Munro G (1997) J Am Ceram Soc 80:1919
11. Pabst W, Gregorova E (2003) J Mater Sci Lett 22:959
12. Phani KK, Niyogi SK (1987) J Mater Sci 22:257
13. Roberts AP, Garboczi EJ (2002) Proc Roy Soc Lond 458:1033